Journal of Colloid and Interface Science 369 (2012) 302–308

Contents lists available at SciVerse ScienceDirect

Journal of Colloid and Interface Science

www.elsevier.com/locate/jcis

Electrooxidation of nitrite on a silica–cerium mixed oxide carbon paste electrode

Gustavo Silveira [a], Andréia de Morais [a], Paulo César Mendes Villis [a], Camila Marchetti Maroneze [b], Yoshitaka Gushikem [b], Alzira Maria Serpa Lucho [a], Fábio Luiz Pissetti [a,*]

[a] Instituto de Química, Universidade Federal de Alfenas, 37130-000 Alfenas, MG, Brazil
[b] Instituto de Química, Universidade Estadual de Campinas, PO Box 6154, 13083-970 Campinas, SP, Brazil

ARTICLE INFO

Article history:
Received 28 June 2011
Accepted 26 November 2011
Available online 6 December 2011

Keywords:
Sol–gel process
Mixed oxide
Silica–ceria
Electrochemical sensor

ABSTRACT

A silica–cerium mixed oxide (SiCe) was prepared by the sol–gel process, using tetraethylorthosilicate and cerium nitrate as precursors and obtained as an amorphous solid possessing a specific surface area of 459 $m^2\ g^{-1}$. Infrared spectroscopy of the SiCe material showed the formation of the Si—O—Ce linkage in the mixed oxide. Scanning electron microscopy/energy dispersive spectroscopy indicated that the cerium oxide particles were homogenously dispersed on the matrix surface. X-ray diffraction and ^{29}Si solid-state nuclear magnetic resonance implied non-crystalline silica matrices with chemical environments that are typical for silica-based mixed oxides. X-ray photoelectron spectroscopy showed that Ce was present in approximately equal amounts of both the 3+ and 4+ oxidation states. Cyclic voltammetry data of electrode prepared from the silica–cerium mixed oxide showed a peak for oxidation of Ce^{3+}/Ce^{4+} at 0.76 V and electrochemical impedance spectroscopy equivalent circuit indicated a porous structure with low charge transfer resistance. In the presence of nitrite, the SiCe electrode shows an anodic oxidation peak at 0.76 V with a linear response as the concentration of the analyte increases from 3×10^{-5} at 3.9×10^{-3} mol L^{-1}.

1. Introduction

Cerium oxide has been widely investigated due the combination of an elevated transport capacity and the ability to shift between reduced and oxidized states. One of the main applications of cerium oxide is as a catalyst for treating exhaust gases from internal combustion engines through the oxidation of hydrocarbons to CO and CO_2 and the reduction of nitrogen oxides to N_2 [1]. Another application that has gained prominence in recent years is the use of cerium oxide in electrodes to construct electrochemical sensors for determination of different analytes [2–4]. Cerium oxide presents low thermal stability and undergoes sintering at high temperatures changing important properties [5]. One approach to overcome this problem is inserting the oxide in a silica matrix, which confers the necessary mechanical and thermal resistance without loose the other properties [6].

To achieve this combination of silica–cerium oxide, the sol–gel process is a useful method, since it uses hydrolysis and condensation reactions to form a polymeric network that can be converted into the oxide of interest through the removal of the liquid components. This is a very versatile technique for the synthesis of mixed oxides because it allows production of highly homogeneous solids using relatively mild conditions [7]. Use of the sol–gel process for preparing materials containing cerium oxide covers a broad spectrum of applications such as formation of electrochromic devices [8], coating of aluminum alloys [9], and catalysts for the oxidation of CO [10].

Nitrite is an important chemical species of both biological and environmental interest due to environmental contamination of the aquifer reservoirs by the infiltration of agricultural fertilizers. For instance, when ingested, this species can bind to hemoglobin, causing methemoglobinemia in infants [11,12]. Many methods have been developed for the detection of nitrite using various techniques such as capillary electrophoresis, chemiluminescence, fluorescence spectroscopy, and high-performance liquid chromatography; however, some of them require complicated and expensive instrumentation. Nitrite anions behave as an electroactive species when exposed to different electrodes, a property that has attracted much interest for the development of electrochemical sensors for its quantification [13,14]. To present efficiency toward this analyte, usually, an electrode with complex composition is necessary, for instance, containing electrons mediators, carbon nanotubes, and a conductive polymer [15]. To the best of our knowledge, there are no reports in the literature using the silica–cerium mixed oxide for the modification of carbon paste electrodes. Thus, the aim of this work is the synthesis of a porous mixed oxide using the sol–gel process in order to confine and disperse cerium oxide into a silica matrix. The texture,

* Corresponding author. Address: Universidade Federal de Alfenas, Instituto de Química, Rua Gabriel Monteiro da Silva, 700, CEP 37130-000 Alfenas, MG, Brazil. Fax: +55 35 3299 1384.
E-mail address: pissetti@unifal-mg.edu.br (F.L. Pissetti).

0021-9797
doi:10.1016/j.jcis.2011.11.060

local structure, and electrochemical properties of the mixed oxides were investigated by X-ray diffraction, infrared spectroscopy, scanning electron microscopy/energy dispersive spectroscopy, ^{29}Si solid-state nuclear magnetic resonance, X-ray photoelectron spectroscopy, cyclic voltammetry, and electrochemical impedance spectroscopy techniques. The material was then used to prepare carbon paste electrodes for the electrooxidation of nitrite.

2. Experimental

2.1. Preparation of silica–cerium mixed oxide

The silica–cerium mixed oxide was prepared by adding a 3.5 ml solution of 3.5 mol L^{-1} aqueous HCl to a 60 ml solution of 1:1 (v/v) ethanol:tetraethylorthosilicate (TEOS). The mixture was stirred for 3 h at 333 K under an argon atmosphere. After the prehydrolysis step, 2.92 g of $Ce(NO_3)_3{\cdot}6H_2O$ was added, and the mixture was stirred for 2 h at 323 K. An additional 1.7 ml of the 3.5 mol L^{-1} HCl aqueous solution was added, and the mixture was stirred for another 3 h at room temperature. The system was then kept without agitation for over 18 h before slowly evaporating the solvent at 333 K until a gel formed. The product obtained was heated at 393 K for 2 h and 423 K for 45 min. The material was pulverized, washed with 0.1 mol L^{-1} HNO_3, distilled water, and ethanol, and dried under vacuum at 353 K for 6 h. The material obtained will be hereafter designated SiCe.

2.2. Scanning electron microscopy (SEM) and X-ray emission analyses (EDS)

A Jeol JSM T300 scanning electron microscope (SEM), equipped with an energy dispersive spectrometer (EDS) microprobe from NORAN Instruments (model series 2), was used to obtain the micrographs of the materials. The samples were dispersed on double-sided conductive tape placed on a copper support and coated with gold using a Balzer (Med 020) device.

2.3. Specific surface area

The specific surface area was determined by the BET method (S_{BET}) from the physical adsorption of N_2 at 77 K using a Micromeritics model Flowsorb II 2300 instrument connected to a 2300 FC flow controller. Prior to measurement, all the samples were outgassed at approximately 10^{-4} Pa at 373 K for 4 h.

2.4. X-ray diffraction

X-ray diffraction patterns were obtained on a Shimadzu XRD-6000 diffractometer using Cu Kα radiation (λ = 0.154 nm, 40 kV *per* 30 mA) and a sweeping velocity of 2° min^{-1} (units of 2θ).

2.5. Infrared spectroscopy

The infrared spectroscopy spectra FTIR were measured using a Shimadzu IR Prestige-21 spectrometer at room temperature in the range between 4000 and 500 cm^{-1} with a resolution of 2 cm^{-1} and taking 20 scans.

2.6. ^{29}Si nuclear magnetic resonance

The ^{29}Si nuclear magnetic resonance NMR spectra were obtained on a Bruker AC300 spectrometer operating at 59.6 MHz using cross-polarization magic angle spinning (CPMAS). The acquisition time was 50 ms with a relaxation cycle of 20 s and a spectral window of 15×10^3 Hz.

2.7. X-ray photoelectron spectroscopy

The X-ray photoelectron spectroscopy XPS spectra were obtained on a VSW HA-100 spherical analyzer using Al Kα radiation (1486.6 eV). The high-resolution spectra were measured using constant analyzer pass energies of 44 eV, which produced a full width at half-maximum (FWHM) of 1.6 eV for the Au ($4f_{7/2}$) line. The powdered samples were pressed into pellets and fixed to a stainless steel sample holder with double-sided tape and analyzed without further preparation. Curve fitting was performed using Gaussian line shapes, and the Shirley background was subtracted from the data. The pressure during the measurements was always less than 2×10^{-8} mbar. Charging effects were corrected by linearly shifting the spectra so that the C1*s* line had a binding energy of 284.6 eV.

2.8. Electrochemical measurements

The carbon paste electrodes were prepared by mixing 50 mg of silica–cerium with 50 mg of graphite (Fluka) using 15 μL of liquid paraffin as a binder and depositing into a cavity in contact with a platinum disk fused at the end of a 5 mm internal diameter glass tube (designed as SiCe). For comparison, two other electrodes were prepared, one with only graphite (CB) and other with carbon/silica (Silica gel 60 – Merck®) 1:1 m:m (Si), keeping the same conditions of total mass and paraffin amount. An Autolab PGSTAT 128N potentiostat–galvanostat apparatus was used in conjunction with a three electrode system for the voltammetric measurements. All the electrochemical experiments were carried out in an electrochemical cell with 0.5 mol L^{-1} KCl solution as the supporting electrolyte, a saturated calomel electrode (SCE) as the reference electrode, a platinum wire as the counter electrode, and carbon paste as the working electrode.

The impedance experiments were carried out using an Autolab/EchoChimie PGStat 30 apparatus. The results were obtained in a frequency range between 100 kHz and 5 mHz, applying a 5 mV sinusoidal voltage. The equivalent circuit was fitted using the Frequency Response Analyzer (FRA) software. For this study, the SiCe electrode was compared to electrodes with follow compositions: 70 mg SiCe / 30 mg graphite (SiCe70) and 30 mg SiCe / 70 mg of graphite (SiCe30).

The preparation of the solutions and production of the carbon paste electrode were performed immediately before taking the measurements. This procedure was adopted to verify the reproducibility of the measurements, and these studies were carried out three times over three different days.

3. Results and discussion

3.1. Characteristics of the samples

The S_{BET} measurements resulted in a value of 459 $m^2\ g^{-1}$, which indicates that the obtained mixed oxide possesses a porous texture. This value is similar to other mixed oxides prepared trough the sol–gel method [16,17]. Fig. 1 shows the FT-IR spectra of the SiCe and pure SiO_2 materials. The main absorption bands for the SiCe sample were similar to those of pure silica and can be assigned as follows: 1200–1100 cm^{-1} (ν_{as} Si—O—Si), 690 cm^{-1} (ν_s Si—O—Si), and 456 cm^{-1} (δ Si—O—Si) (not shown). The band observed at 973 cm^{-1} for SiO_2 (Fig. 1b) can be assigned to the Si—O stretching mode (νSiO) of the free silanol groups (≡Si—OH). In the case of SiCe, this band is shifted to 947 cm^{-1} (Fig. 1a), indicating the formation of the Si—O—Ce linkage in the mixed oxide and a strong interaction between the silica and ceria phases [17,18].

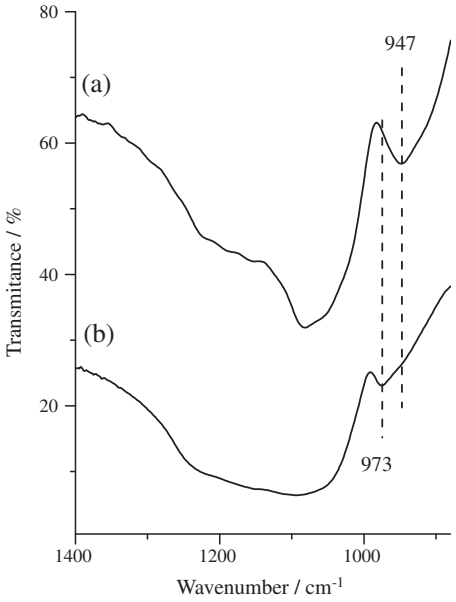

Fig. 1. Infrared spectra for (a) SiCe and (b) SiO_2.

3.2. Scanning electron microscopy (SEM) and X-ray emission analysis (EDS)

Fig. 2 shows the SEM micrographs and the corresponding cerium mapped by EDS (white points) for SiCe. The analyses reveal that the cerium oxide particles are, within the magnification used, homogenously dispersed onto the SiO_2 surface with no detectable phase segregation of the oxide particles in the matrix. This homogeneous dispersion of the metal oxide into the matrix is an important characteristic for the material applications as it enables a uniform distribution of the cerium oxide species on the surface [19].

3.3. X-ray diffraction patterns

Fig. 3 shows the XRD patterns for a sample SiCe. Three peaks can be observed between 40° and 80° in the diffractogram that indicates a low amount of cerium oxide possessing the cubic fluorite crystal structure [20]. This suggests the presence of Ce^{4+} in the material. The vitreous halo between 20° and 30° (2θ) is typical of non-crystalline silica matrices.

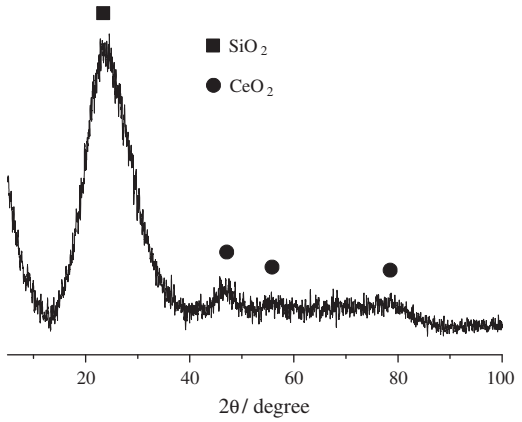

Fig. 3. X-ray diffractogram of SiCe.

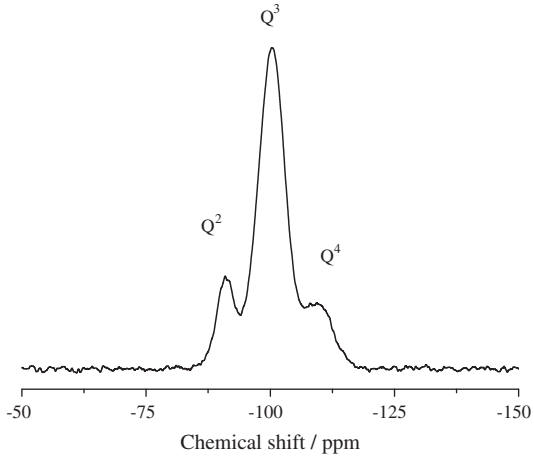

Fig. 4. ^{29}Si NMR spectrum of SiCe.

3.4. ^{29}Si nuclear magnetic resonance

The ^{29}Si NMR spectrum, shown in Fig. 4, contains a set of three signals at −90, −100, and −110 ppm, which can be assigned to groups Q^2, Q^3, and Q^4 units, respectively. The chemical shift values for the silicon atoms in this distinct chemical environment are in good agreement with those found in literature for silica-based materials prepared by the sol–gel method [16,18,21].

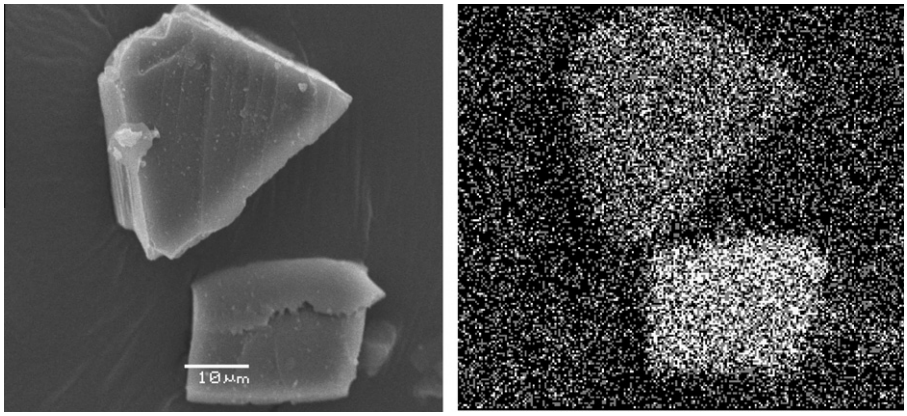

Fig. 2. Images of SiCe material obtained by SEM and EDS for cerium atoms.

Table 1
XPS binding energies from the Ce 3d spectrum of SiCe and from Ce^{3+}/Ce^{4+} standards found in literature.

Sample	Bind energies (eV)									
	Ce ($3d_{5/2}$)					Ce ($3d_{3/2}$)				
	v^0	v	v'	v''	v'''	u^0	u	u'	u''	u'''
SiCe	881.3	–	884.5	887.6	897.4	899.7	–	902.8	905.3	–
CeO_2[a]	–	882.6	–	889.3	898.6	–	900.8	–	907.8	916.7
$Ce(acac)_3$[a]	881.4	–	885.2	–	–	899.5	–	903.6	–	–
Ce_2O_3[b]	880.9	–	885.3	–	–	899.7	–	903.8	–	–

$Ce(acac)_3$ = cerium (III) acetylacetonate.
[a] Ref. [31].
[b] Ref. [32].

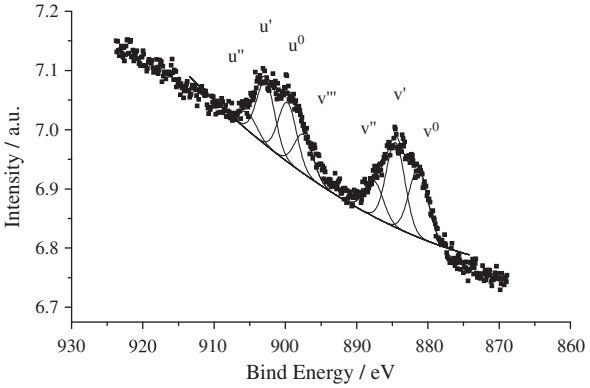

Fig. 5. XPS spectrum of the SiCe material for the 3d level of cerium. The u and v peaks were assigned as discussed in the text. ■ are experimental results and – is the best fit.

3.5. X-ray photoelectron spectroscopy

The results of the XPS analysis of the Ce 3d level are presented in Table 1 and Fig. 5. The XPS spectrum of CeO_2 3d level can be described by using three spin-orbit doublets, the $3d_{3/2}$ and $3d_{5/2}$, referred to as u and v, respectively. The doublets u''' and v''' result from a final electron configuration of Ce $3d^9\ 4f^0$ (O $2p^6$). The lower energy states, u, v, and u'', v'', result from the final electron configurations of Ce $3d^9\ 4f^1$(O $2p^5$) and Ce $3d^9\ 4f^2$(O $2p^4$), respectively [17,22–26]. The two pairs of spin-orbit doublets (u', v' and u^0, v^0) from Ce^{3+} arise from the different configurations of the 4f final state, which is strongly hybridized with the oxygen 2p orbitals. The peaks u' and v' are characteristic of an electronic configuration of $3d^9\ 4f^1$ (O $2p^6$) for Ce^{3+}, and the peaks u^0 and v^0 are the result of an electronic configuration of $3d^9\ 4f^2$ (O $2p^5$) for Ce^{3+} [24,26–28]. The spectrum also shows peaks related to Ce^{4+} (v'', u'', and v''') and the other characteristic peaks of Ce^{3+} compounds (v^0, v', u^0, and u'). These results are consistent with the literature values [29].

Analysis of the integrated areas of these peaks can provide a semi-quantitative ratio of Ce^{3+} in this material, as described elsewhere [26–28,32–34], and indicates that the amount is approximately 75%. However, the reduction of cerium ions during XPS analysis has been widely reported in the literature [30,32,35] and must be considered. The rate of photoreduction decreases as a function of the irradiation time. After 300 min of irradiation, it is estimated that ~30% of Ce^{4+} undergoes reduction [30]. Taking these factors into consideration, approximately 50% of cerium in the SiCe material may be present in the 3+ oxidation state and 50% in the 4+ oxidation state. The observed differences in binding energy when compared to the tabulated values are related to the distortion that the silica network causes in ceria due to the formation of Si—O—Ce bonds.

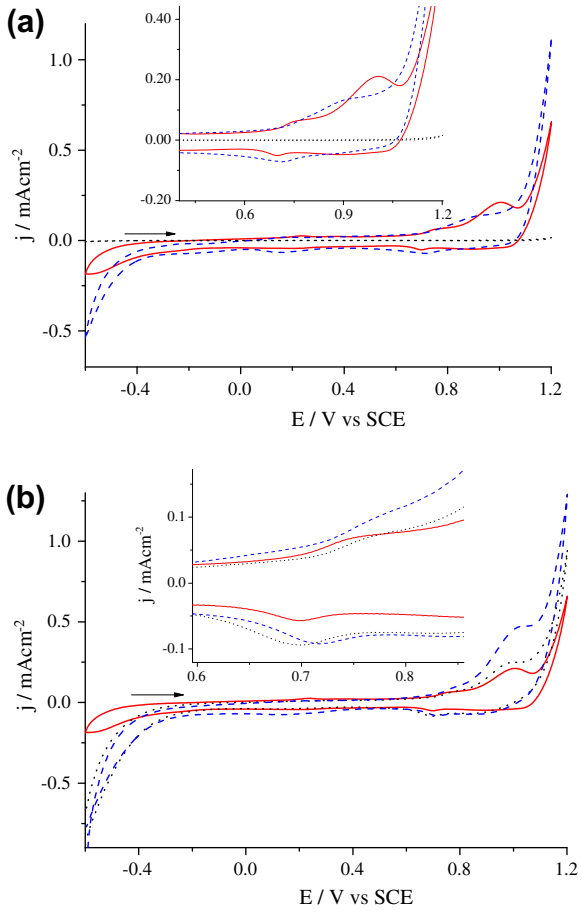

Fig. 6. (a) Cyclic voltammograms of CB (dot line), Si (dash line), and SiCe (solid line) electrodes and (b) SiCe30 (dot line), SiCe50 (solid line), and SiCe70 (dash line) in KCl at a concentration of 0.5 mol L^{-1}. The scan rate was 50 mV s^{-1}.

The photoelectron peak for the Si 2p component was observed at 104 eV, and the 1s level of the oxygen was observed at 532.6 eV in the SiCe material (graphs not shown). These values are similar to those found in the literature [6], with small differences in the binding energy occurring due to the chemical environment [17,6].

3.6. Electrochemical properties of the material

From cyclic voltammograms of SiCe carbon paste electrode was not observed a significant difference when in acidic media or KCl (not shown). Since the nitrite electrooxidation was detected in KCl, the electrochemical studies were conducted at a neutral pH,

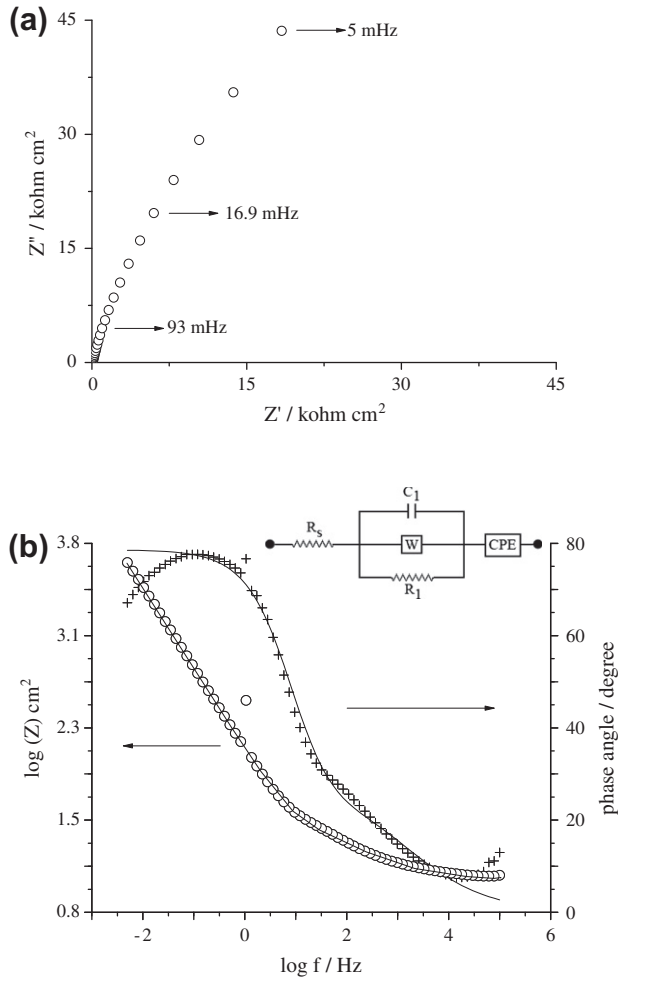

Fig. 7. (a) Nyquist and (b) Bode diagrams with experimental (○ and +) and simulated data (—) for a SiCe electrode in KCl with a concentration of 0.5 mol L^{-1}. An open circuit potential equal to 0.198 V was observed. The equivalent circuit is inserted.

which can be considered an advantage since do not demand a controlled pH to detect nitrite.

Fig. 6a) shows the cyclic voltammograms of the CB, Si, and SiCe carbon paste electrodes. The electrode CB does not presented peaks. Si electrode presents one broad peak at 0.9 V, anodic scan, probably due cationic characteristics of SiO_2 [3,36]. In the electrode containing SiCe, this process occurs at 1.0 V and the shift occurs probably due the interaction of cerium with the silica in the mixed oxide. The other anodic peak on SiCe electrode at 0.76 V, which presented an increase of current density when higher amount of SiCe material was added in carbon paste electrode (Fig. 6b), can be related to Ce^{3+}/Ce^{4+} oxidation [37–40].

Electrochemical impedance spectroscopy was employed to determine the charge transfer resistance (R_{tc}) and the equivalent circuit, of the SiCe carbon paste electrode. Fig. 7 presents the impedance plots of the complex plane (a) and the Bode diagram (b).

Table 2
Values for the electrical components of the equivalent circuit.

Element	R_s (Ω cm^2)	C_1 (pF cm^{-2})	R_1 (Ω cm^2)	W (Ω^{-1} cm^{-2})	Q (F cm^2)	n
Value	17.24	1.32	48.18	1.03×10^{-3}	2.58×10^{-4}	0.87

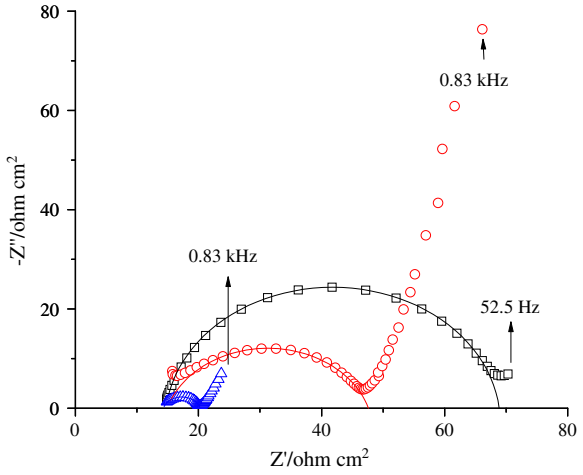

Fig. 8. Nyquist diagram and simulation of semicircles for the △ SiCe70, ○ SiCe and □ SiCe30 electrodes in KCl with a concentration of 0.5 mol L^{-1} in 5×10^{-3} mol L^{-1} $[Fe(CN)_6]^{3-}$ solution. The applied potential was 0.245 V vs. SCE.

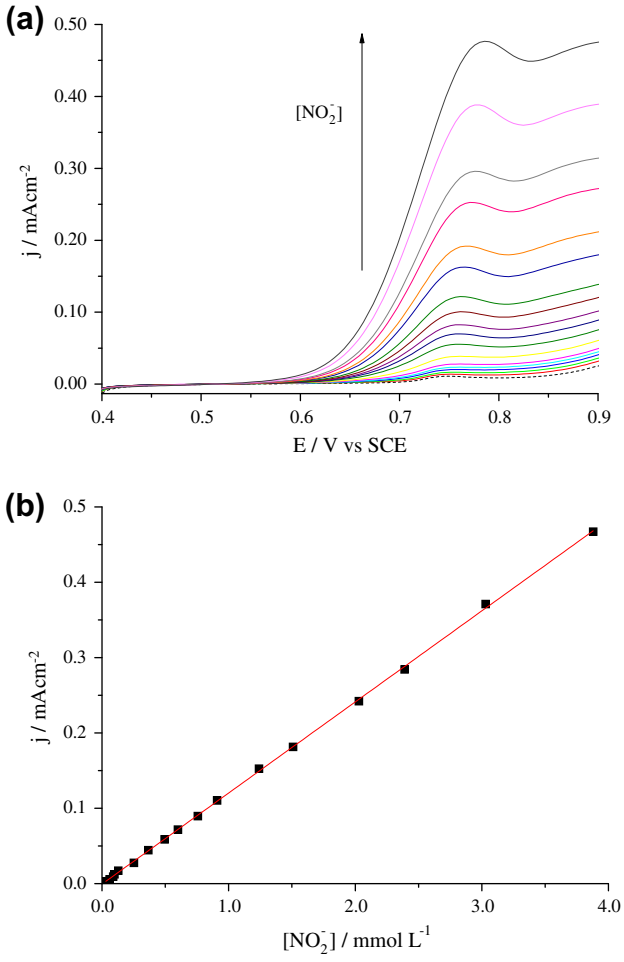

Fig. 9. (a) Linear sweep voltammetry of SiCe in the presence of $NaNO_2$ with concentration ranging from 3×10^{-5} to 3.9×10^{-3} mol L^{-1} (dashed line without nitrite). KCl 0.5 mol L^{-1}. The scan rate was 20 mV s^{-1} and (b) anodic peak current versus nitrite concentration. (Blank was subtracted.)

The obtained results are characteristic for systems that have a time constant at low frequencies and a phase angle of around 75°, indicating a capacitive behavior [41]. However, there is also an observed time constant at the intermediate frequencies of 10–300 Hz related to the diffusional processes [42].

Table 3
Comparison between determination range, scan rate, and peak potential of different electrodes for nitrite sensing.

Electrode	Determination range (mmol L^{-1})	Scan rate (mV s^{-1})	Peak potential (V)	Refs.
SiO_2/SnO_2/C-graphite/ $(SiPy+)_4CoPcTs^{4-}$	0.04–1.7	20	0.84 (SCE)	[45]
SiO_2/SnO_2/phosphate/ CoP	0.6–1.0	20	0.72 (SCE)	[46]
c/l-Cys/P3MT/ MWCNT/GCE	0.1–0.2	25	0.78 (Ag/ AgCl)	[47]
G4-NH4/MWNT	0.1–1.5	100	0.78 (SCE)	[13]
SiCe	0.03–3.9	20	0.76 (SCE)	

Fig. 7b shows the Bode diagram of the experimental data and a simulation of the equivalent circuit (EC). The resistor R_s represents the solution resistance, R1 is the material resistance, and C1 is the double layer capacitance due the charge rearrangement at electrode-solution interface. W is the impedance to mass transfer (Warburg impedance), which was included in the EC to account for the diffusional processes occurring in the system. The deviation from an ideal solid-state capacitor is strongly related to the electrode surface, e.g., roughness, degree of crystallinity, and the adsorption of ions. This deviation from ideal capacitive behavior was represented by the constant phase element (CPE), and the equivalent circuit data are presented in Table 2. The value obtained for the elements indicated an electrode with porous structure and low electrical resistance [41].

Fig. 8 shows the Nyquist diagrams of SiCe70, SiCe and SiCe30 materials in a $[Fe(CN)_6]^{3-}$ solution. The charge transfer resistance was determined from the intersection of the semicircle with the real axis of the Nyquist diagrams in high frequencies region.

Charge transfer resistance, R_{tc}, was calculated from $R_{tc} = R_p - R_s$. For Sice30, SiCe, and SiCe70, the obtained values were 53, 32, and 6 $\Omega\,cm^2$, respectively. For an increasing amount of SiCe material in the carbon paste electrode, the R_{tc} decreases, suggesting that Ce^{3+}/Ce^{4+} redox plays an important role on the electrode, favoring the electron transfer [41,43].

3.7. Electrochemical applications

In order to evaluate the electrooxidation of the carbon paste electrode toward nitrite oxidation, linear sweep voltammetry was obtained both in the absence and with increasing concentrations of the analyte (Fig. 9a). For the electrooxidation of nitrite, there was not significant variation with increasing amount of cerium oxide in the carbon paste electrode. An anodic oxidation peak was observed at 0.76 V and increases proportionally with the nitrite concentration.

The plot of the anodic oxidation peak current against NO_2^- concentration in Fig. 9b shows a linear correlation between $R^2 = 0.9997$ and $n = 17$, with a concentration range of 3×10^{-5} to 3.9×10^{-3} mol L^{-1} of nitrite. The detection limit was calculated following IUPAC recommendations [44], and the value obtained was 2×10^{-6} mol L^{-1}.

The linear range observed for SiCe electrode is similar to that obtained for others systems where it is necessary to use electron mediators, such as phthalocyanines and porphyrines [45,46] or even more complex materials [13,47] (Table 3). Another contribution of the work was to obtain a similar limit of detection in KCl media, compared to others materials where is necessary a controlled pH [13,47]. It may be noted that the carbon paste electrode containing SiCe possesses a good reproducibility when applied to the electrooxidation of nitrite. Electrocatalytic effect of the material can be attributed to free cerium coordination sites and the redox coupling of Ce^{3+}/Ce^{4+}.

4. Conclusions

A simple route for the synthesis of a mixed silica–cerium oxide by sol–gel has been described. The results showed the cerium oxide was homogeneously dispersed throughout the silica matrix. X-ray diffraction showed that the oxides are in the amorphous state. The binding energies of the cerium 3d level suggested that the both the 3+ and 4+ oxidation states of the cerium ions are present in roughly equal amounts.

The low charge transfer resistance demonstrated that the material shows a high rate of electron transfer at the electrode surface. The observed electrooxidation of nitrite on the carbon paste electrode made from SiCe material was satisfactory, demonstrating a directly proportional response between the current and the nitrite concentration in KCl media, suggesting the possibility of developing an analytical method for the quantification of this analyte through electrochemical sensing.

Acknowledgments

Gustavo Silveira and Andreia de Morais acknowledge CAPES and UNIFAL-MG for providing financial support through a masters scholarships. Paulo Villis thanks FAPEMIG and Camila Maroneze is indebted to CNPq for providing a Post-Doctoral fellowship. Authors Alzira Lucho and Fábio Pissetti are indebted to FAPEMIG while CNPq and Yoshitaka Gushikem are indebted to FAPESP for financial support. We also technical assistance from R.C.G. Vinhas.

References

[1] A. Trovarelli, M. Boaro, E. Rocchini, C. de Leitenburg, G. Dolcetti, J. Alloys Compd. 323–324 (2001) 584.
[2] Y. Wei, M. Li, S. Jiao, Q. Huang, G. Wang, B. Fang, Electrochim. Acta 52 (2006) 766.
[3] A. Gupta, N. Prabhakar, R. Singh, A. Kaushik, B.D. Malhotra, Thin Solid Films 519 (2010) 1122.
[4] D. Zhang, W. Wu, X. Ni, X. Cao, X. Zhang, X. Xu, S. Li, G. Han, A. Ying, Z. Tong, J. Mater. Sci. 44 (2009) 3344.
[5] B. Reddy, A. Khan, Catal. Surv. Asia 9 (2005) 155.
[6] A.A.S. Alfaya, Y. Gushikem, S.C.d. Castro, Microporous Mesoporous Mater. 39 (2000) 57.
[7] G. Frenzer, W.F. Maier, Annu. Rev. Mater. Res. 36 (2006) 281.
[8] C. Avellaneda, M. Berton, L. Bulhoes, Sol. Energy Mater. Sol. Cells 92 (2008) 240.
[9] H. Hasannejad, M. Aliofkhazraei, A. Shanaghi, T. Shahrabi, A.R. Sabour, Thin Solid Films 517 (2009) 4792.
[10] M. Thammachart, V. Meeyoo, T. Risksomboon, S. Osuwan, Catal. Today 68 (2001) 53.
[11] P. Miao, M. Shen, L. Ning, G. Chen, Y. Yin, Anal. Bioanal. Chem. 399 (2011) 2407.
[12] S. Rajesh, A.K. Kanugula, K. Bhargava, G. Ilavazhagan, S. Kotamraju, C. Karunakaran, Biosens. Bioelectron. 26 (2010) 689.
[13] N. Zhu, Q. Xu, S. Li, H. Gao, Electrochem. Commun. 11 (2009) 2308.
[14] Y. Zhang, L. Luo, Y. Ding, L. Li, Microchim. Acta 167 (2009) 123.
[15] C.-Y. Lin, A. Balamurugan, Y.-H. Lai, K.-C. Ho, Talanta 82 (2010) 1905.
[16] M.E. Manriquez, T. Lopez, R. Gomez, J. Sol-Gel Sci. Technol. 26 (2003) 853.
[17] F.L. Pissetti, M.S.P. Francisco, R. Landers, Y. Gushikem, J. Braz. Chem. Soc. 18 (2007) 976.
[18] S.C. Laha, P. Mukherjee, S.R. Sainkar, R. Kumar, J. Catal. 207 (2002) 213.
[19] E.S. Ribeiro, S.L.P. Dias, S.T. Fujiwara, Y. Gushikem, R.E. Bruns, J. Appl. Electrochem. 33 (2003) 1069.
[20] X. Song, N. Jiang, Y. Li, D. Xu, G. Qiu, Mater. Chem. Phys. 110 (2008) 128.
[21] A. van Blaaderen, A. Vrij, J. Colloid Interface Sci. 156 (1993) 1.
[22] E. Stoyanova, D. Guergova, D. Stoychev, I. Avramova, P. Stefanov, Electrochim. Acta 55 (2010) 1725.
[23] P. Burroughs, A. Hamnett, A.F. Orchard, G. Thornton, Dalton Trans. (1976) 1686.
[24] E. Bêche, P. Charvin, D. Perarnau, S. Abanades, G. Flamant, Surf. Interface Anal. 40 (2008) 264.
[25] J. Gasserramirez, B. Dunn, D. Ramirez, E. Fillerup, G. Turpin, Y. Shi, R. Ernst, R. Pugmire, E. Eyring, K. Pettigrew, J. Non-Cryst. Solids 354 (2008) 5509.
[26] Z. Xu, L. He, Y. Zhao, R. Mu, S. He, X. Cao, J. Alloys Compd. 491 (2010) 729.
[27] M.S.P. Francisco, V.R. Mastelaro, P.A.P. Nascente, A.O. Florentino, J. Phys. Chem. B 105 (2001) 10515.

[28] S. Deshpande, S. Patil, S.V.N.T. Kuchibhatla, S. Seal, Appl. Phys. Lett. 87 (2005) 133113.
[29] J.Z. Shyu, W.H. Weber, H.S. Gandhi, J. Phys. Chem. 92 (1988) 4964.
[30] P.W. Park, J.S. Ledford, Langmuir 12 (1996) 1794.
[31] E. Paparazzo, G.M. Ingo, N. Zacchetti, J. Vac. Sci. Technol. A-Vac. Surf. Films 9 (1991) 1416.
[32] B. Ernst, L. Hilaire, A. Kiennemann, Catal. Today 50 (1999) 413.
[33] A. Laachir, V. Perrichon, A. Badri, J. Lamotte, E. Catherine, J.C. Lavalley, J. El Fallah, L. Hilaire, F. Le Normand, E. Quemere, G.N. Sauvion, O. Touret, J. Chem. Soc., Faraday Trans. 87 (1991) 1601.
[34] E.J. Preisler, O.J. Marsh, R.A. Beach, T.C. McGill, J. Vac. Sci. Technol. B 19 (2001) 1611.
[35] P.-O. Larsson, A. Andersson, J. Catal. 179 (1998) 72.
[36] M. Jaafariasl, E. Shams, M.K. Amini, Electrochim. Acta 56 (2011) 4390.
[37] V. Devadoss, M. Noel, K. Jayaraman, C. Ahmed Basha, J. Appl. Electrochem. 33 (2003) 319.
[38] Y. Wei, B. Fang, T. Arai, M. Kumagai, J. Appl. Electrochem. 35 (2005) 561.
[39] S. Sharma, M.S. Hegde, J. Chem. Phys. 130 (2009) 114706.
[40] T. Chen, K. Yeh, K. Huang, J. Hazard. Mater. 152 (2008) 922.
[41] E. Marafon, A.M.S. Lucho, M.S.P. Francisco, R. Landers, Y. Gushikem, J. Braz. Chem. Soc. 17 (2006) 1605.
[42] L.T. Arenas, D.S.F. Gay, C.C. Moro, S.L.P. Dias, D.S. Azambuja, T.M.H. Costa, E.V. Benvenutti, Y. Gushikem, Microporous Mesoporous Mater. 112 (2008) 273.
[43] W.S. Cardoso, M.S.P. Francisco, A.M.S. Lucho, Y. Gushikem, Solid State Ionics 167 (2004) 165.
[44] J. Mocak, A.M. Bond, S. Mitchell, G. Scollary, Pure Appl. Chem. 69 (1997) 297.
[45] J. Arguello, H.A. Magosso, R. Landers, Y. Gushikem, J. Electroanal. Chem. 617 (2008) 45.
[46] W.S. Cardoso, Y. Gushikem, J. Electroanal. Chem. 583 (2005) 300.
[47] M. Eguílaz, L. Agüí, P. Yáñez-Sedeño, J.M. Pingarrón, J. Electroanal. Chem. 644 (2010) 30.